

Figure 1—Panoramic view of mafic dykes intruding alkali-rich rocks along the southwestern part of the volcanic sequence. (Traverse no. 1A)

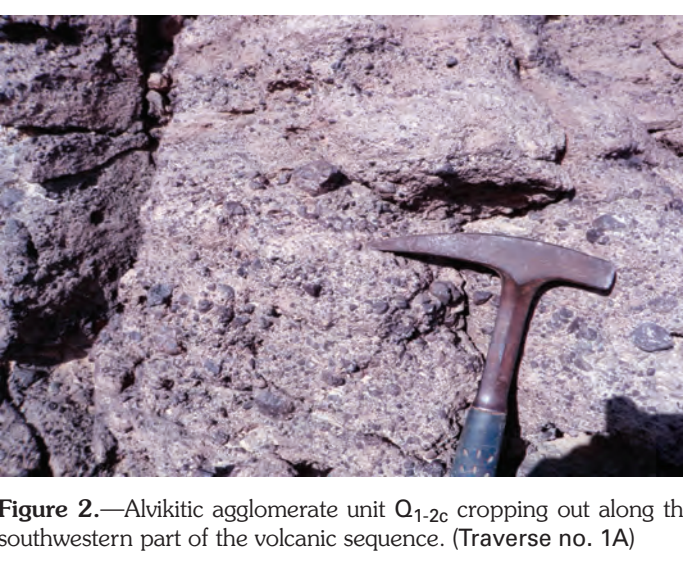


Figure 2—Alkali-rich rocks along the southwestern part of the volcanic sequence. (Traverse no. 1A)



Figure 3—Magnetite-bearing ophiolite, alkali-rich rocks along the southwestern part of the volcanic sequence. (Traverse no. 1A)

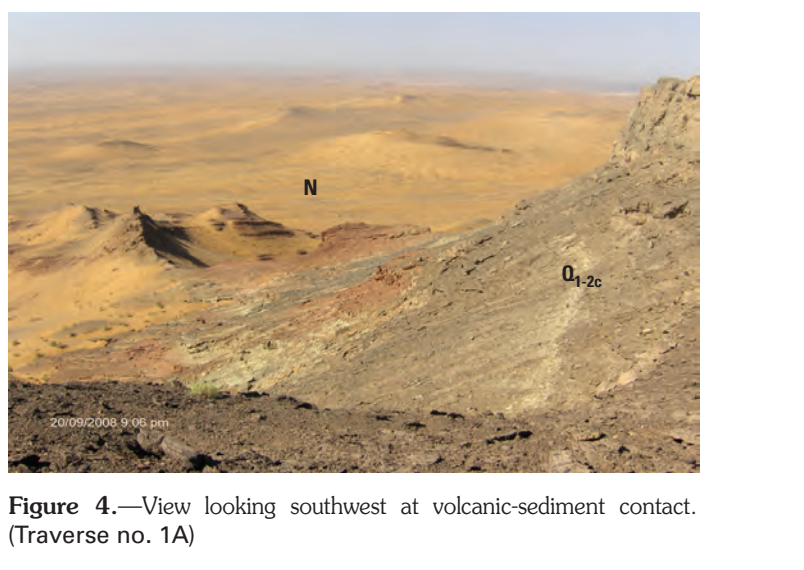


Figure 4—View looking southeast at volcanic-sediment contact. (Traverse no. 1A)

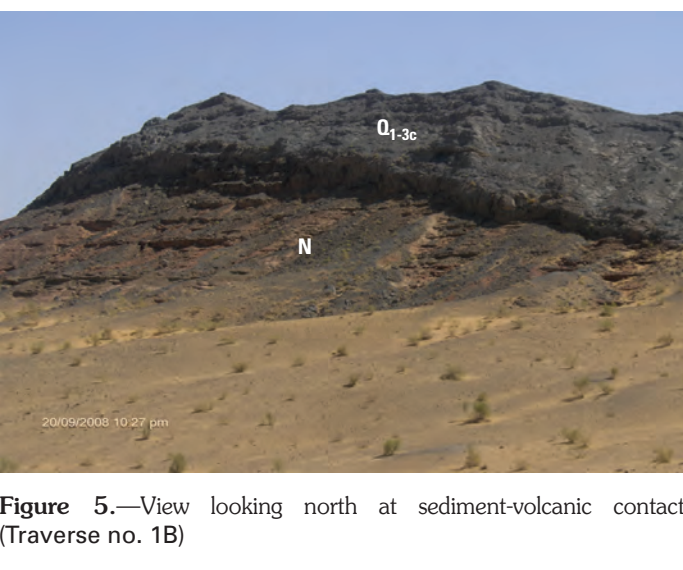


Figure 5—View looking north at sediment-volcanic contact. (Traverse no. 1B)



Figure 6—View of volcanic vent margin on southern part of the Khanneshin carbonate complex, looking southeast. (Traverse no. 1A)

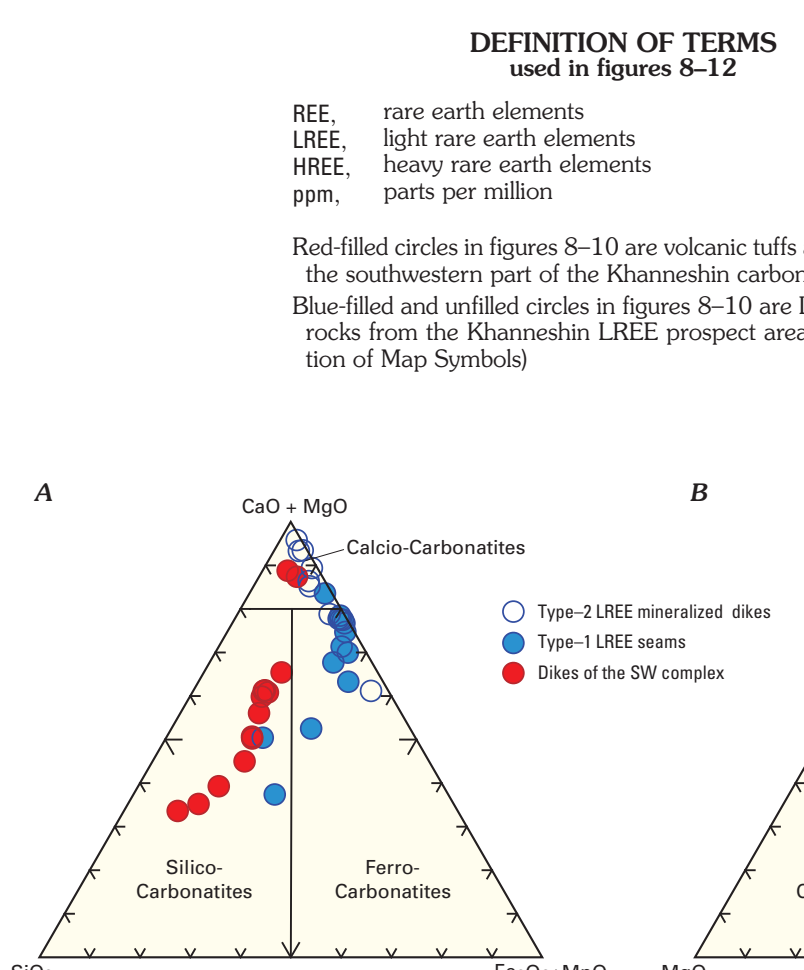


Figure 8A, B—Ternary diagrams of USGS whole-rock geochemical data for the Khanneshin carbonate complex. Diagram A shows SiO₂ vs. Na₂O+K₂O vs. CaO+MgO, and Diagram B shows SiO₂ vs. Na₂O+K₂O vs. CaO+MgO. Both diagrams show data points for various rock types and their distribution within the complex.

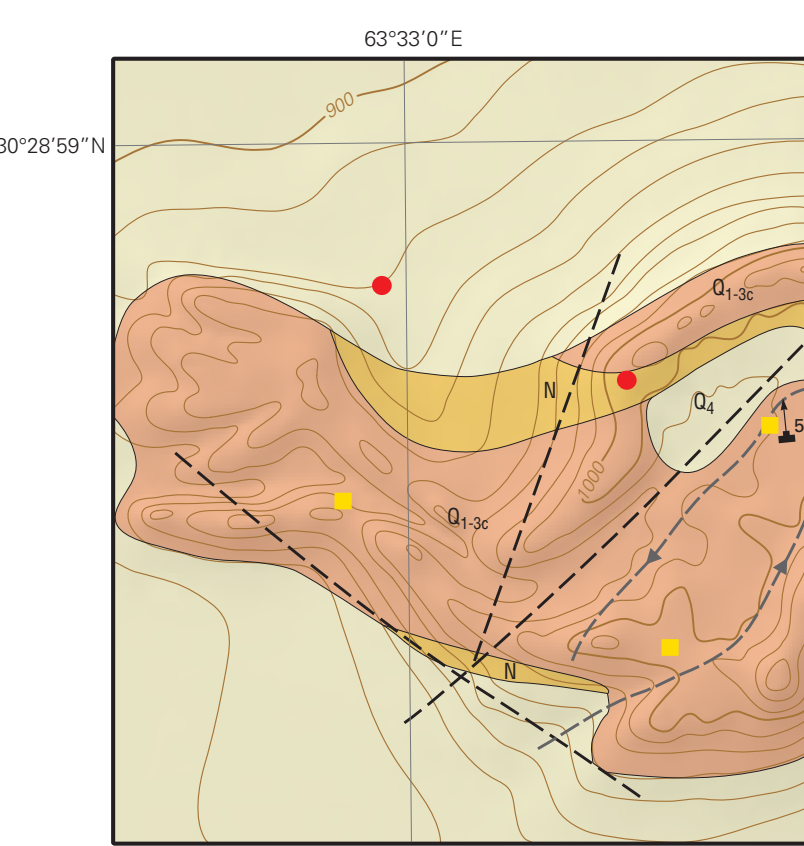


Figure 9A—Variation diagram of Ba (ppm) versus Si (ppm) for the Khanneshin carbonate complex. The diagram shows a clear trend of increasing Ba with increasing Si, indicating a magmatic-hydrothermal origin.

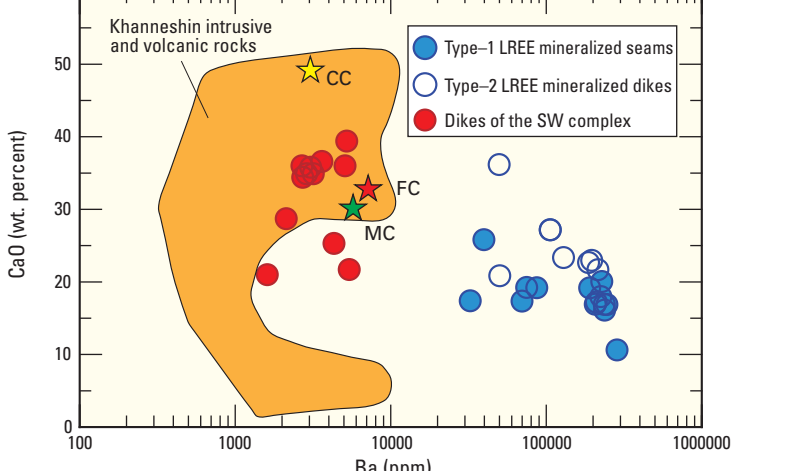


Figure 9B—Variation diagram of Ba (ppm) versus Si (ppm) for the Khanneshin carbonate complex. The diagram shows a clear trend of increasing Ba with increasing Si, indicating a magmatic-hydrothermal origin.

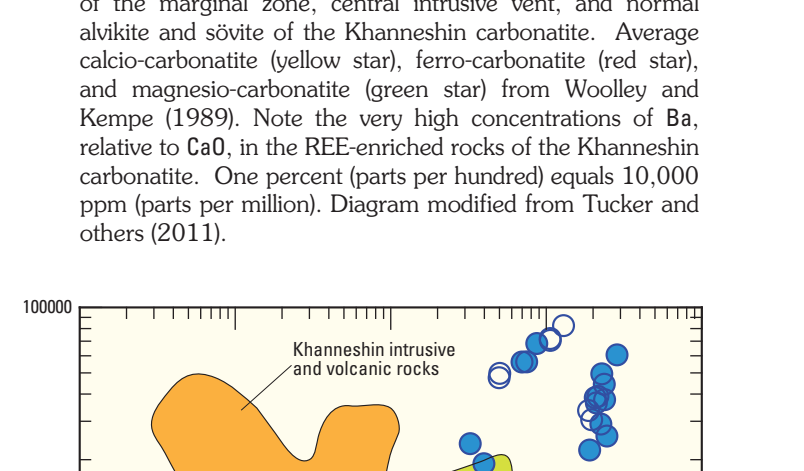


Figure 9C—Variation diagram of Ba (ppm) versus Si (ppm) for the Khanneshin carbonate complex. The diagram shows a clear trend of increasing Ba with increasing Si, indicating a magmatic-hydrothermal origin.

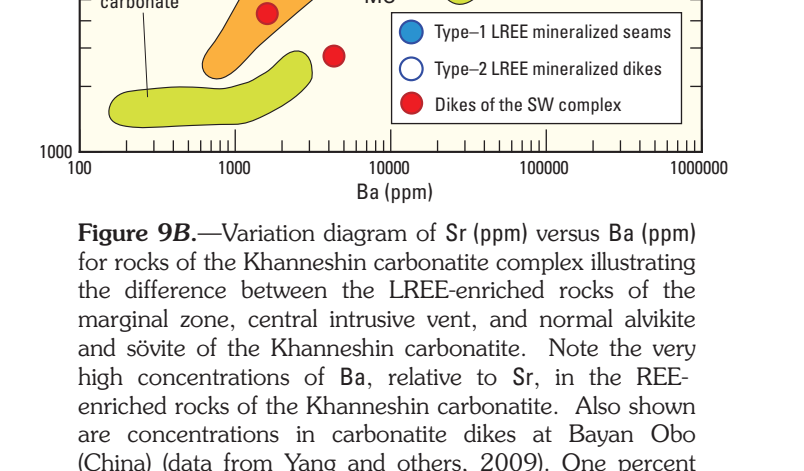


Figure 9D—Variation diagram of Ba (ppm) versus Si (ppm) for the Khanneshin carbonate complex. The diagram shows a clear trend of increasing Ba with increasing Si, indicating a magmatic-hydrothermal origin.

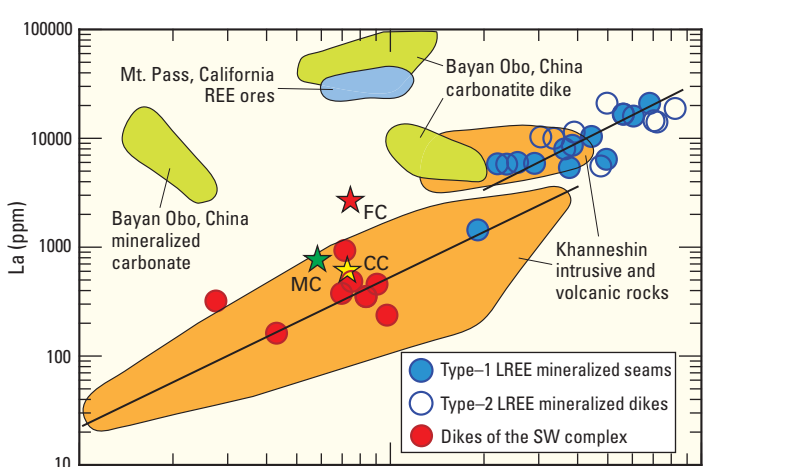


Figure 9E—Variation diagram of Ba (ppm) versus Si (ppm) for the Khanneshin carbonate complex. The diagram shows a clear trend of increasing Ba with increasing Si, indicating a magmatic-hydrothermal origin.

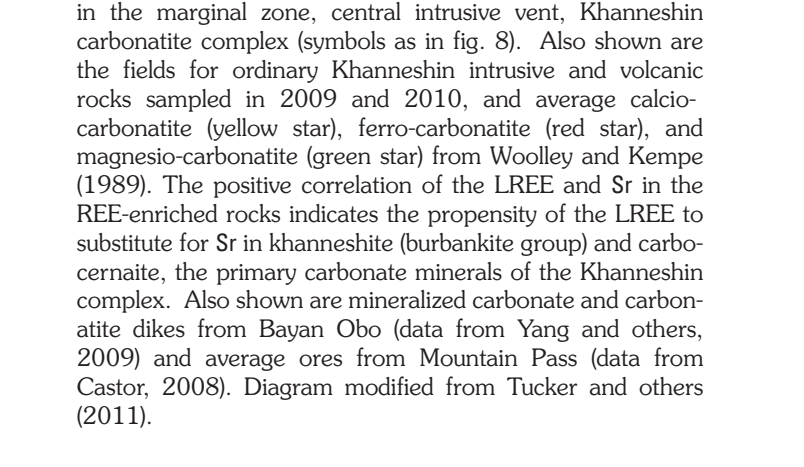


Figure 9F—Variation diagram of Ba (ppm) versus Si (ppm) for the Khanneshin carbonate complex. The diagram shows a clear trend of increasing Ba with increasing Si, indicating a magmatic-hydrothermal origin.

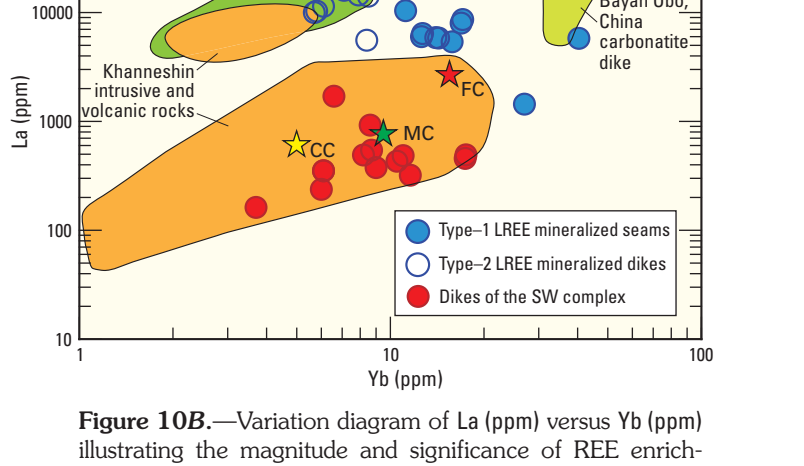


Figure 9G—Variation diagram of Ba (ppm) versus Si (ppm) for the Khanneshin carbonate complex. The diagram shows a clear trend of increasing Ba with increasing Si, indicating a magmatic-hydrothermal origin.

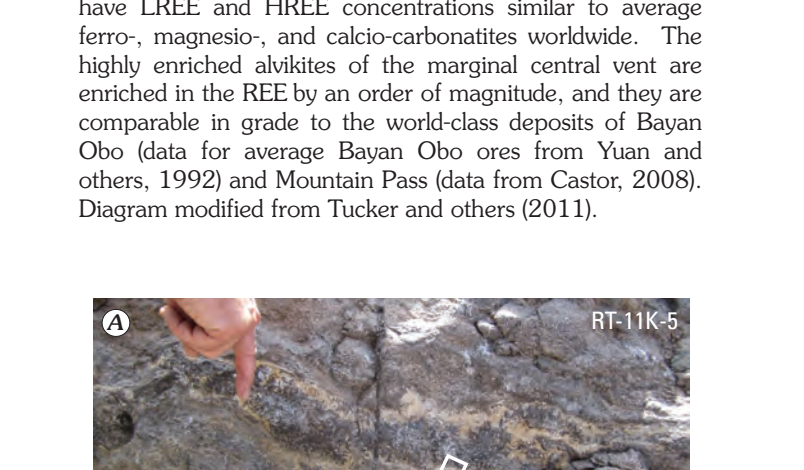


Figure 9H—Variation diagram of Ba (ppm) versus Si (ppm) for the Khanneshin carbonate complex. The diagram shows a clear trend of increasing Ba with increasing Si, indicating a magmatic-hydrothermal origin.

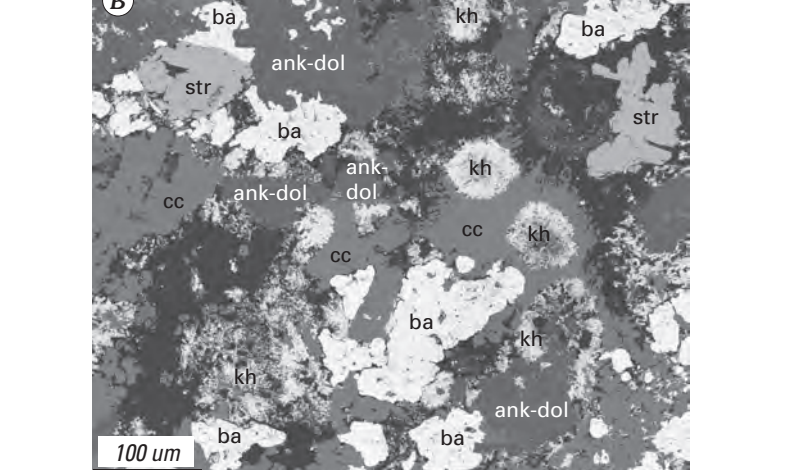


Figure 9I—Variation diagram of Ba (ppm) versus Si (ppm) for the Khanneshin carbonate complex. The diagram shows a clear trend of increasing Ba with increasing Si, indicating a magmatic-hydrothermal origin.

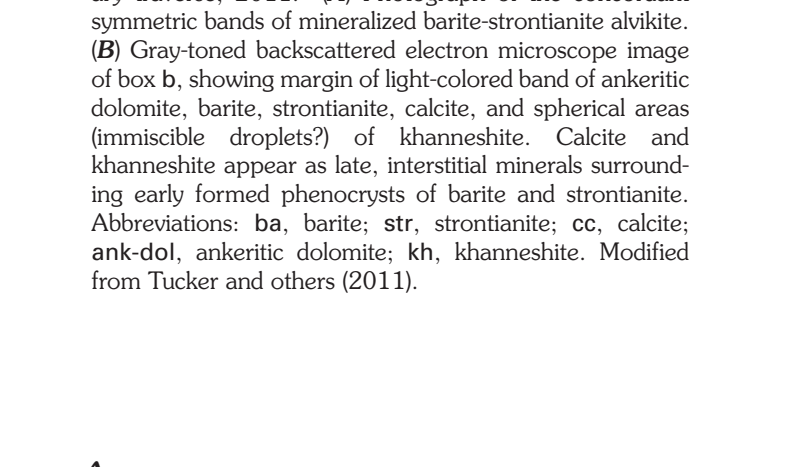


Figure 9J—Variation diagram of Ba (ppm) versus Si (ppm) for the Khanneshin carbonate complex. The diagram shows a clear trend of increasing Ba with increasing Si, indicating a magmatic-hydrothermal origin.

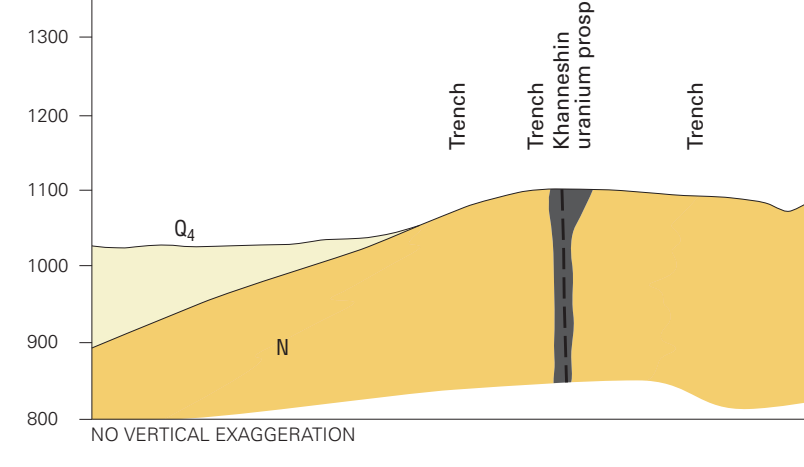


Figure 9K—Variation diagram of Ba (ppm) versus Si (ppm) for the Khanneshin carbonate complex. The diagram shows a clear trend of increasing Ba with increasing Si, indicating a magmatic-hydrothermal origin.

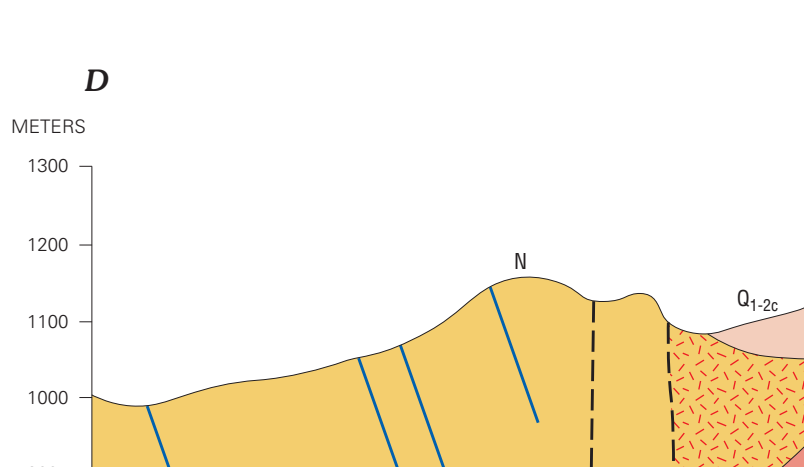


Figure 9L—Variation diagram of Ba (ppm) versus Si (ppm) for the Khanneshin carbonate complex. The diagram shows a clear trend of increasing Ba with increasing Si, indicating a magmatic-hydrothermal origin.



Figure 9M—Variation diagram of Ba (ppm) versus Si (ppm) for the Khanneshin carbonate complex. The diagram shows a clear trend of increasing Ba with increasing Si, indicating a magmatic-hydrothermal origin.

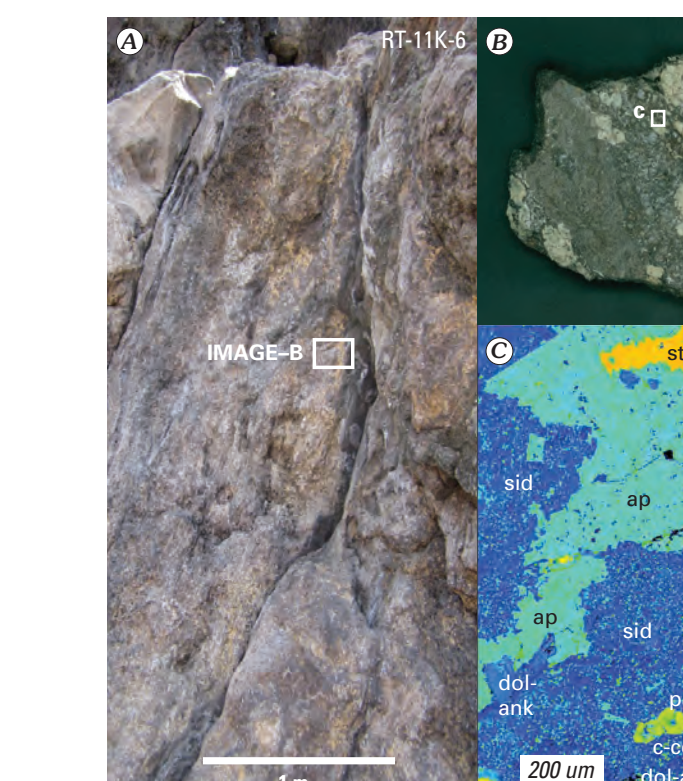


Figure 10—Map of the Khanneshin carbonate complex showing the distribution of various rock types and their relationships. The map includes a legend and a scale bar.

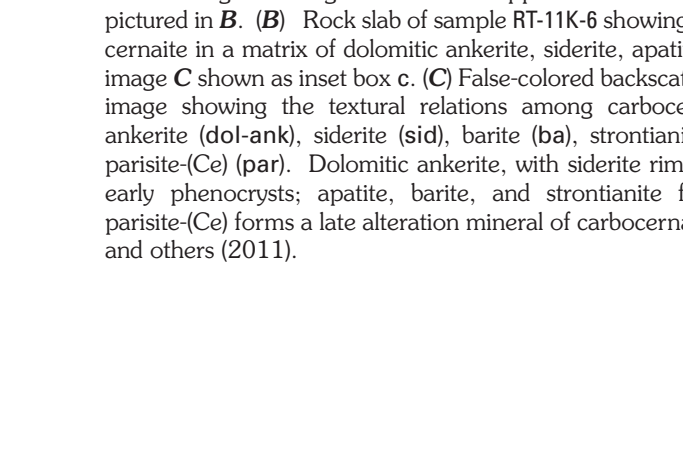


Figure 11—Map of the Khanneshin carbonate complex showing the distribution of various rock types and their relationships. The map includes a legend and a scale bar.

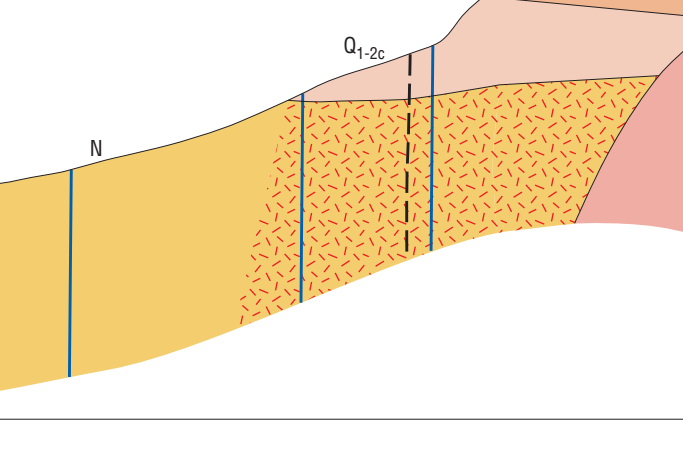


Figure 12—Map of the Khanneshin carbonate complex showing the distribution of various rock types and their relationships. The map includes a legend and a scale bar.

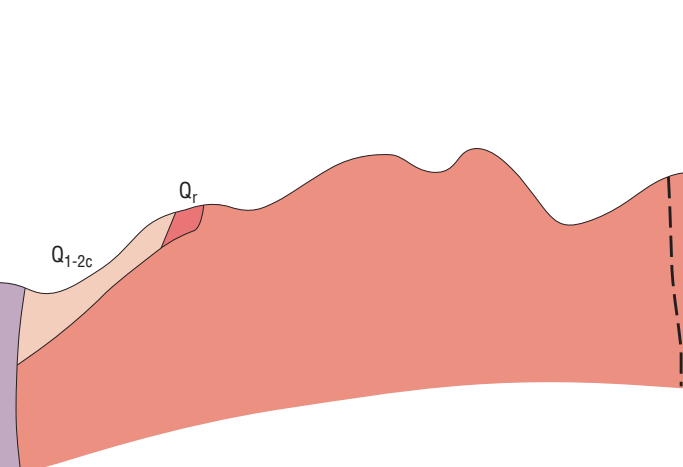


Figure 13—Map of the Khanneshin carbonate complex showing the distribution of various rock types and their relationships. The map includes a legend and a scale bar.



Figure 14—Map of the Khanneshin carbonate complex showing the distribution of various rock types and their relationships. The map includes a legend and a scale bar.



Figure 7—View of layered igneous rocks (basalt) along the southwestern part of the volcanic sequence. (Traverse no. 1A)

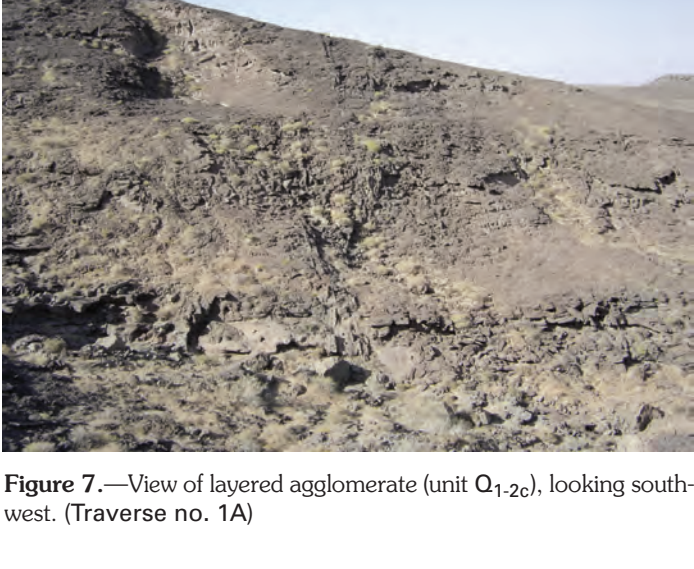


Figure 15—View looking southeast from the northern margin of the central intrusive vent, Khanneshin carbonate complex. (Traverse no. 3)



Figure 16—View looking west across the northern margin of the central intrusive vent, Khanneshin carbonate complex. (Traverse no. 3)

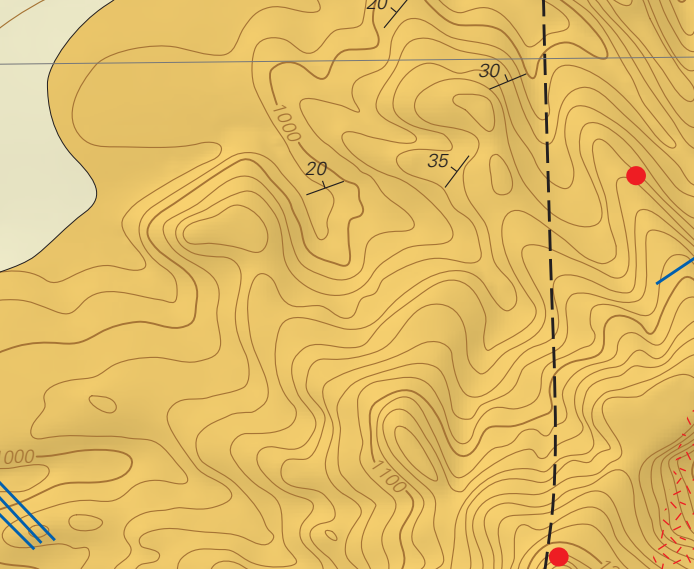


Figure 17—Close-up view of another Type 1 interbedded with an intrusive mass of fine-grained basalt, calcite, and dolomite. (Traverse no. 3)

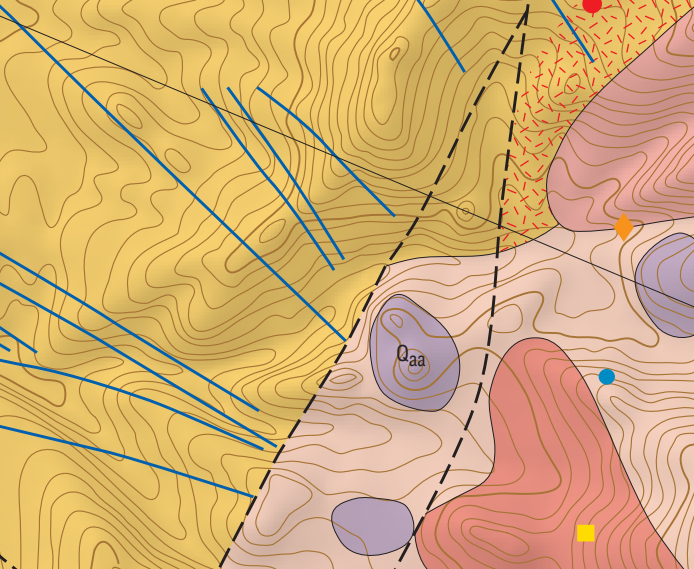


Figure 18—Tabular sheet, approximately 1.5 m thick, outlined by dashed line, of typical Type 2 interbedded showing very coarse-grained rare earth element (REE) enriched carbonate cutting finely bedded dolomite in the northeastern margin of the central intrusive vent. (Traverse no. 3)

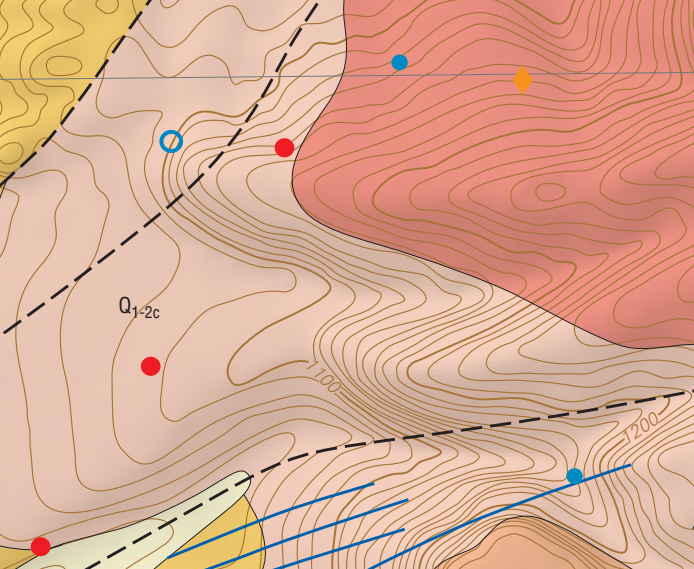


Figure 19—Close-up view of Type 2 interbedded in a coarse-grained carbonate dike. Note the coarse-grained igneous texture with dolomite crystals of barite, barite, and calcite, and the presence of dolomite, barite, and calcite. (Traverse no. 3)

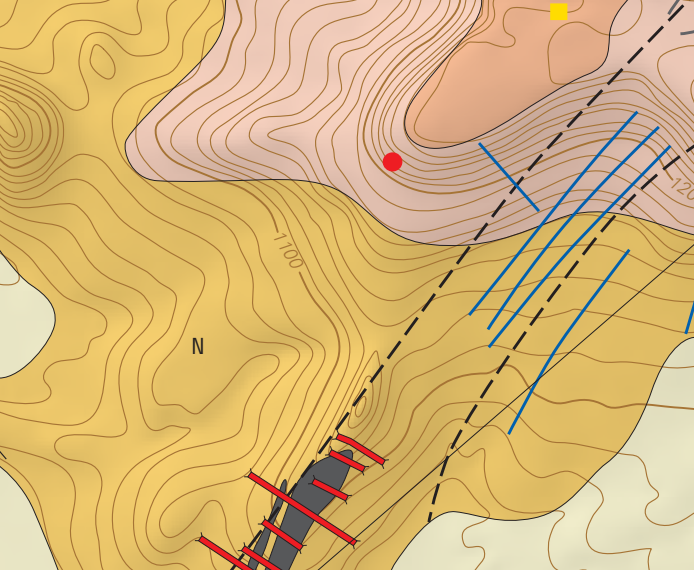


Figure 20—Close-up view of barite and dolomite (dolomite) in a granitic patch of Type 2 interbedded tabular sheet shown in Figure 18. Other visible interbeds include barite, barite, and calcite. (Traverse no. 3)

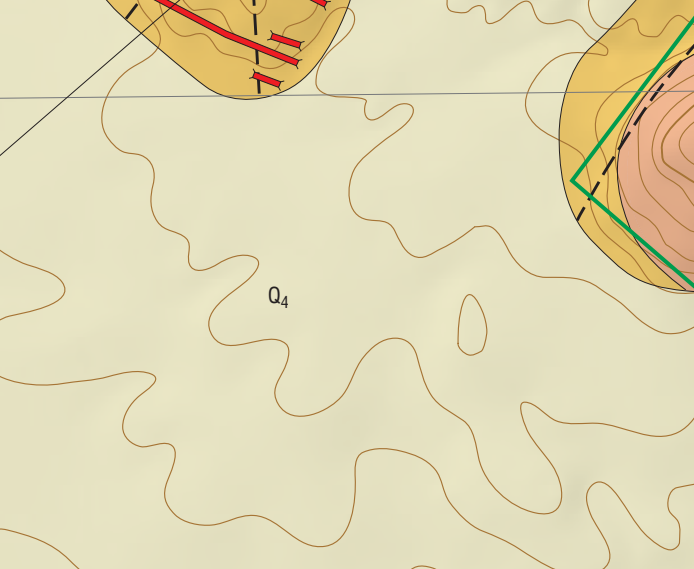


Figure 21—Hydrothermally altered rare earth element (REE) minerals of the Type 1 veins and disseminated pods in barite-sulfate dolomite, northeastern margin of the central intrusive vent. (Traverse no. 3)

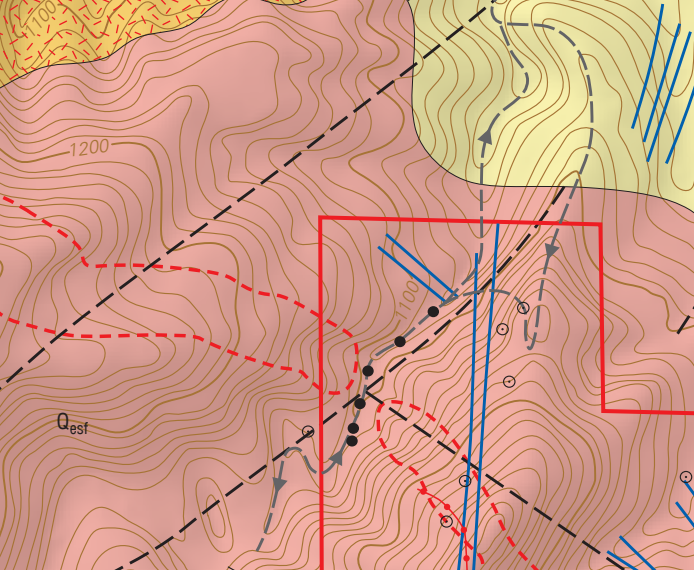
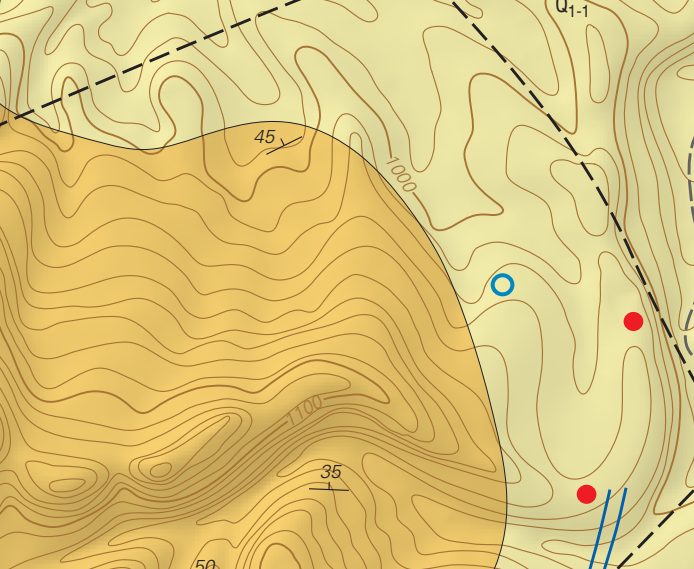
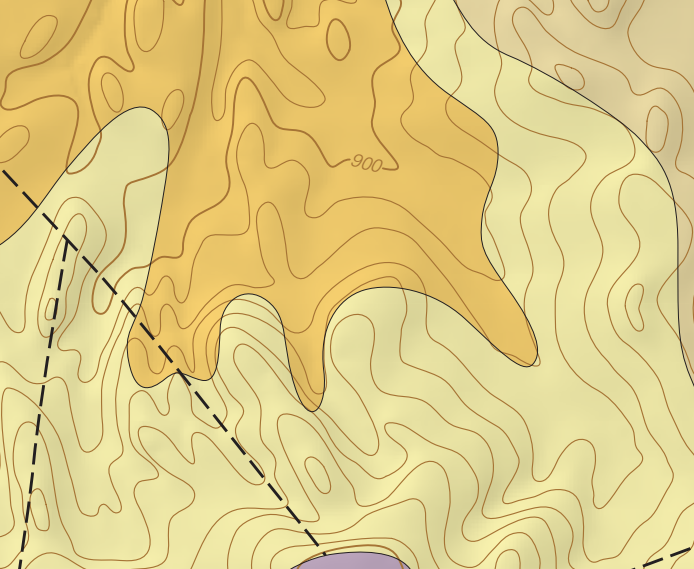
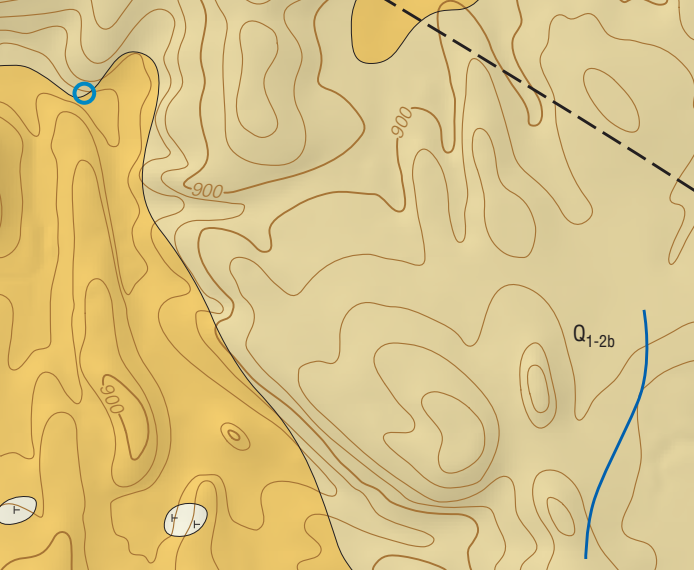
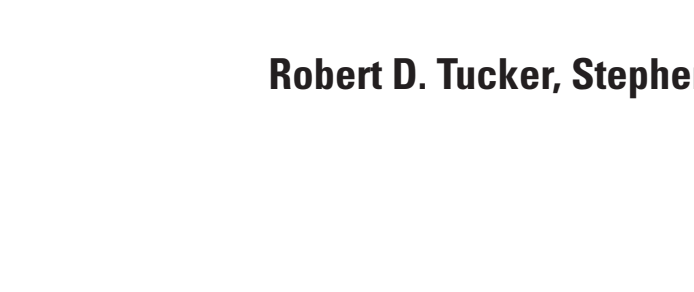
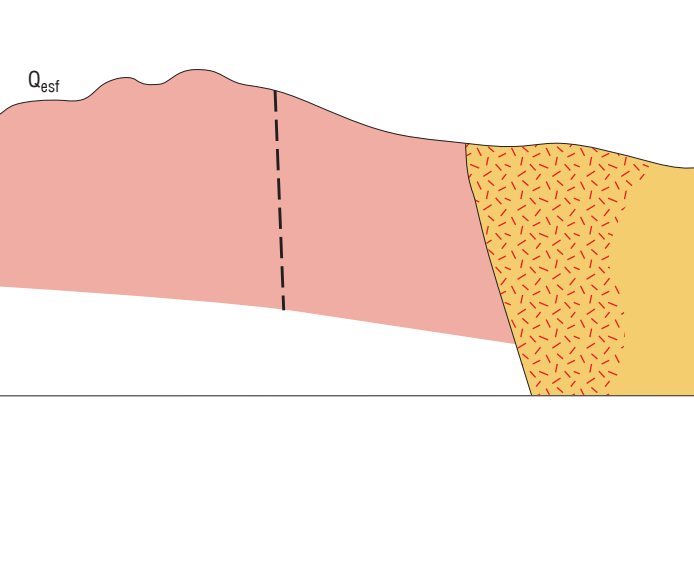
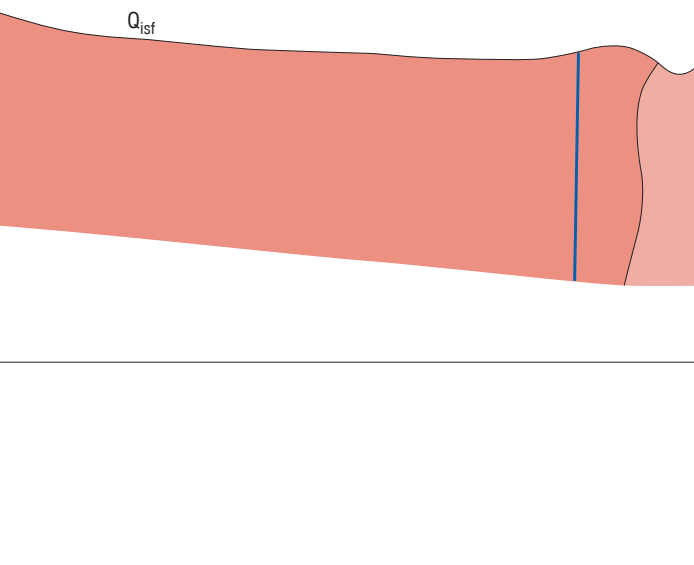
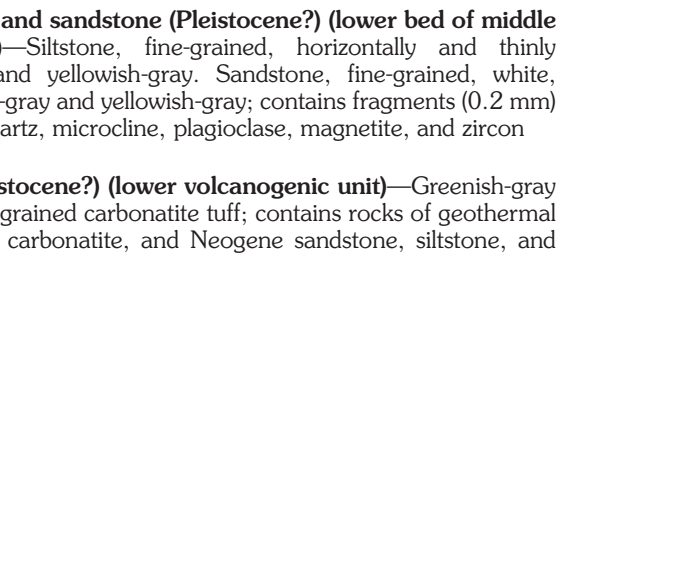
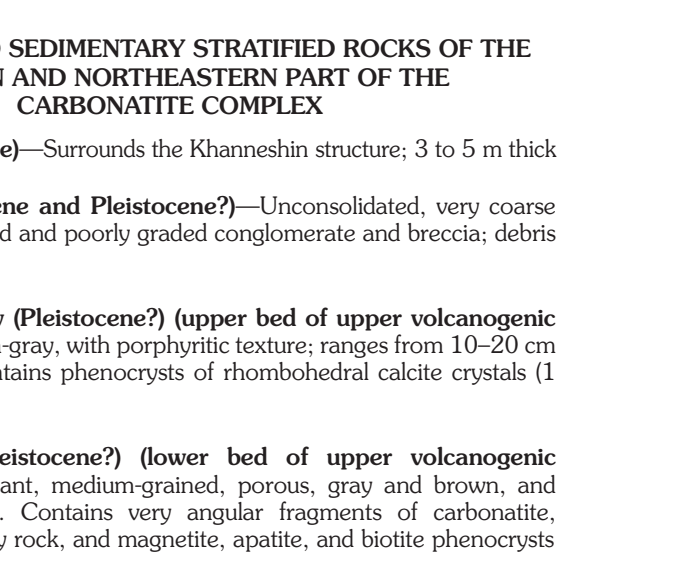
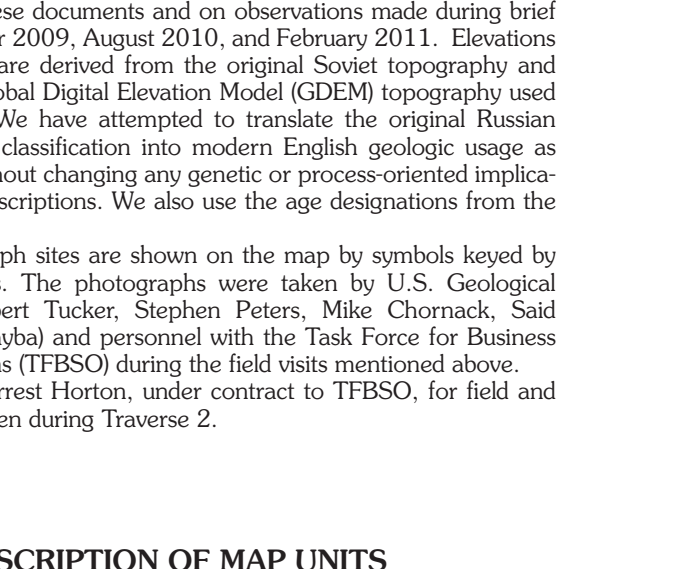
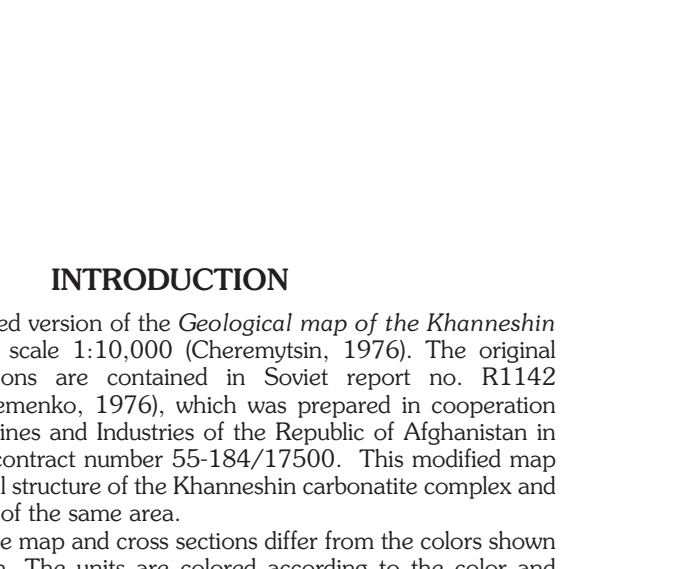
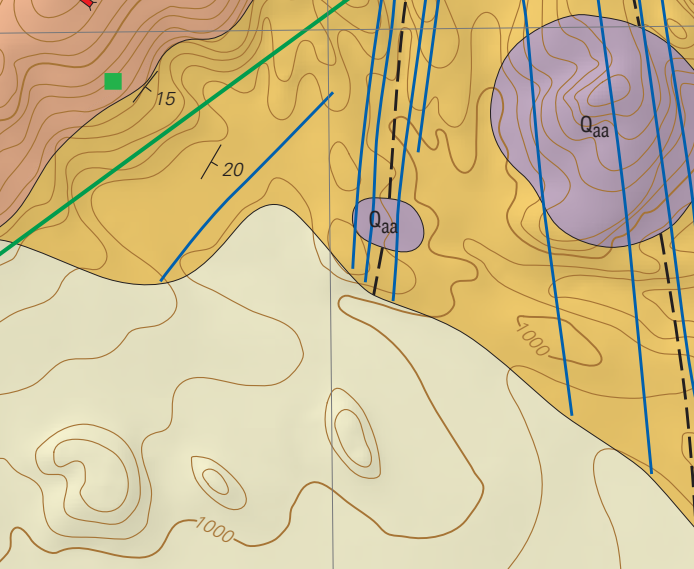
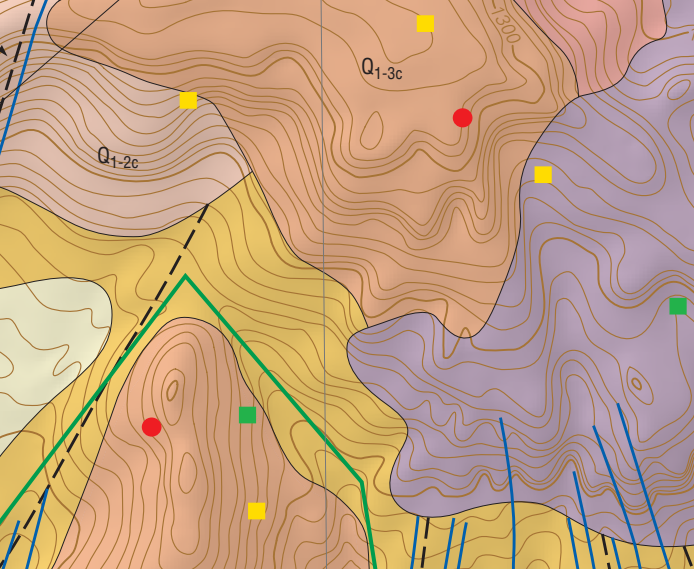
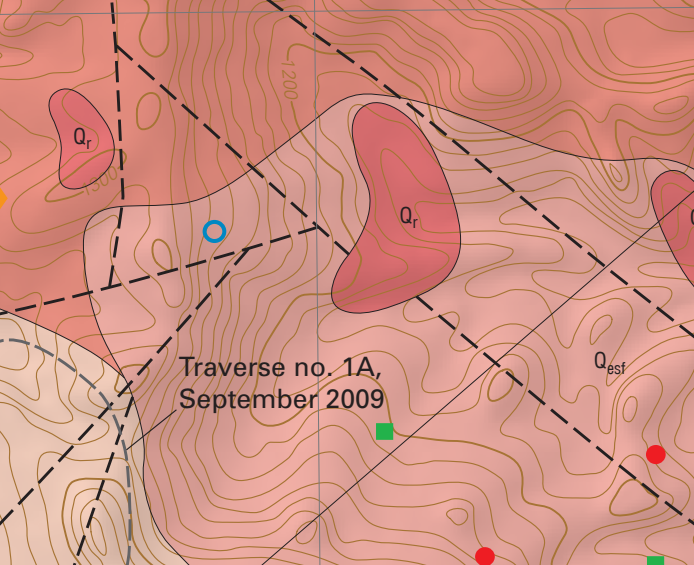
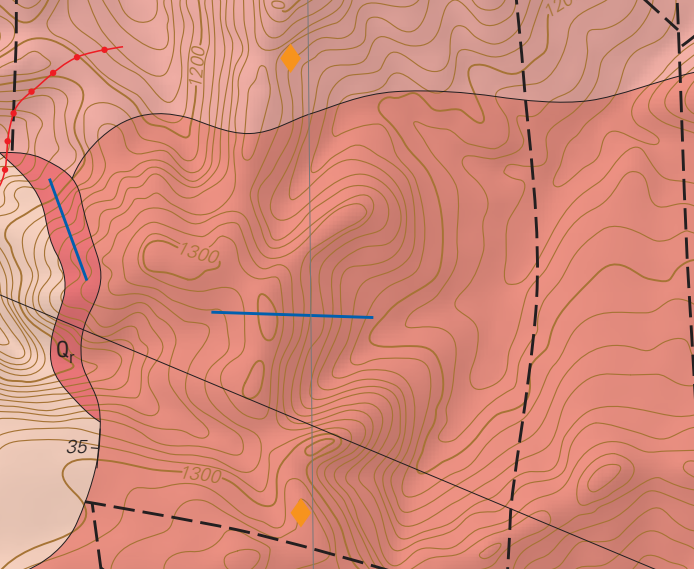
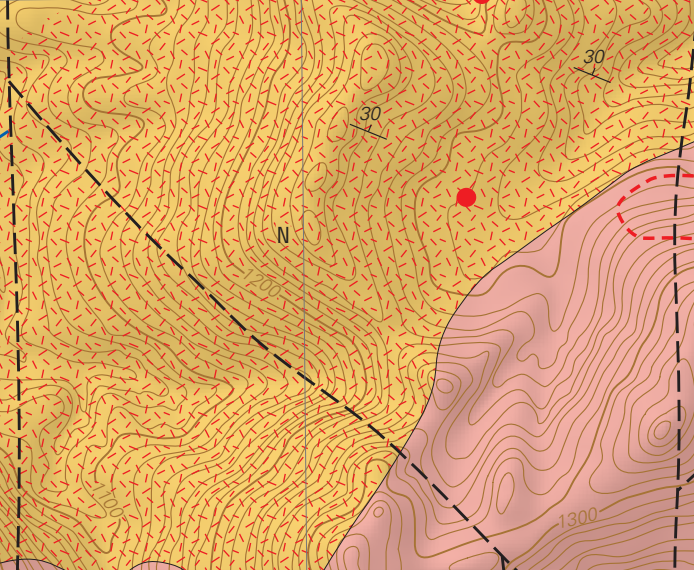
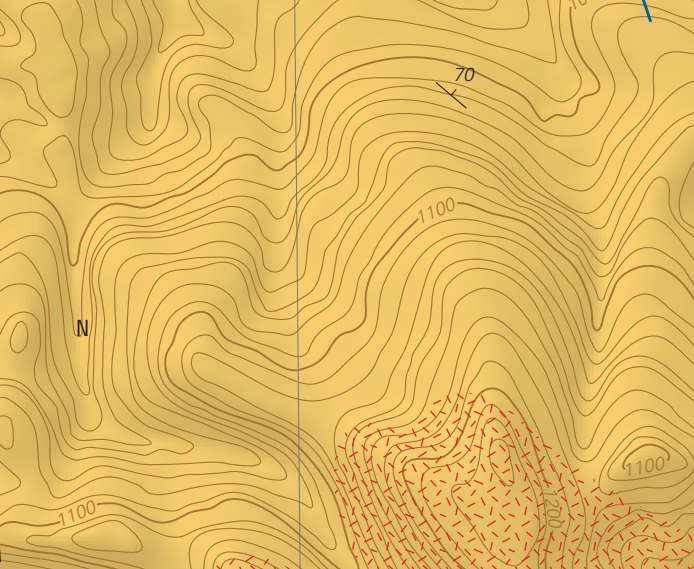
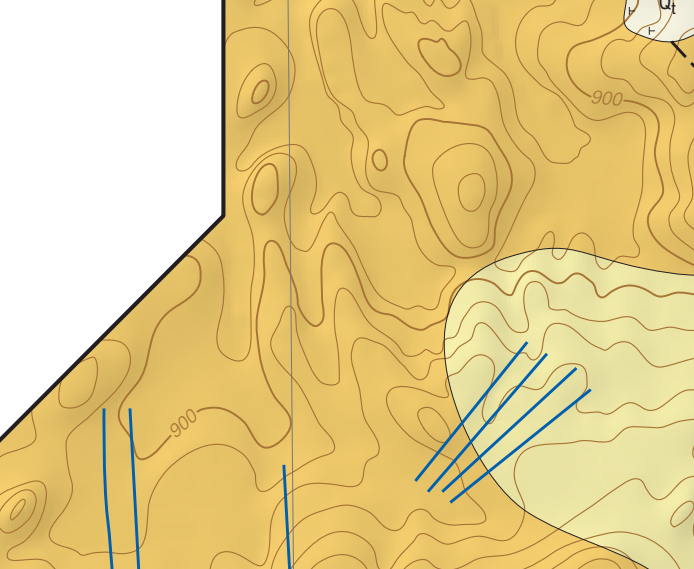
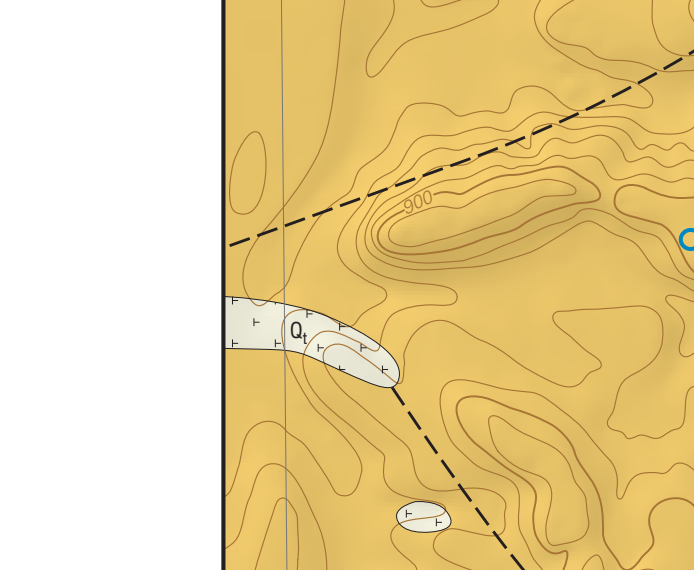
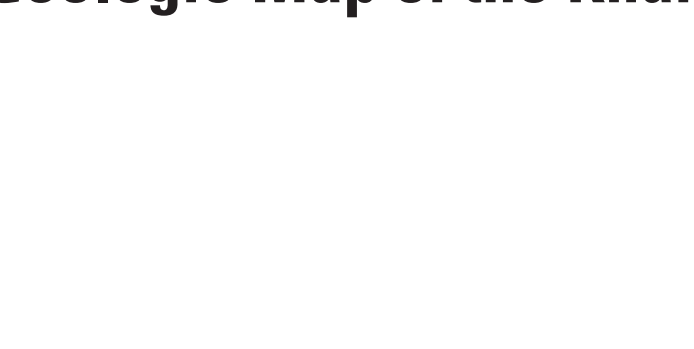
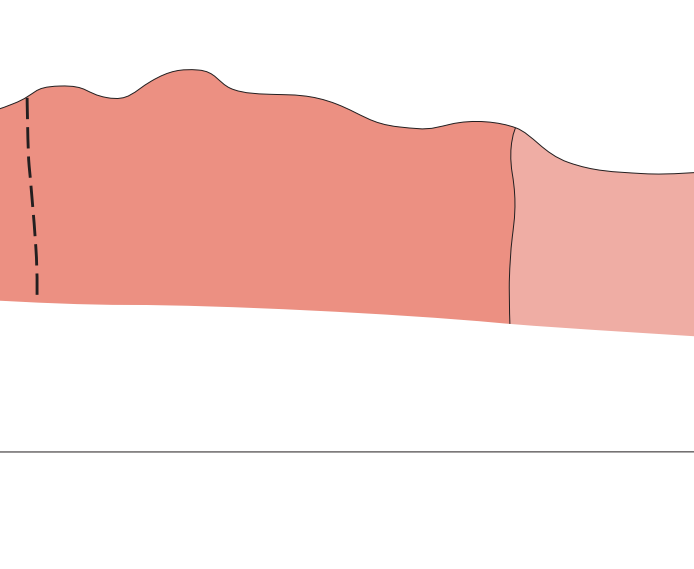
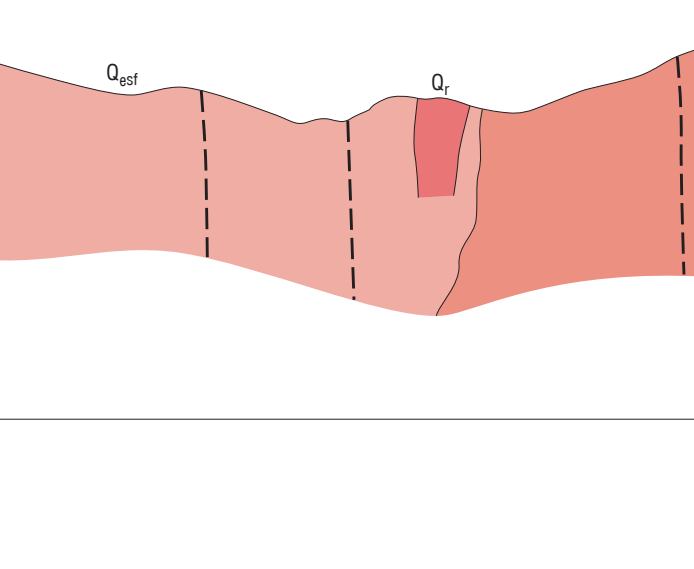
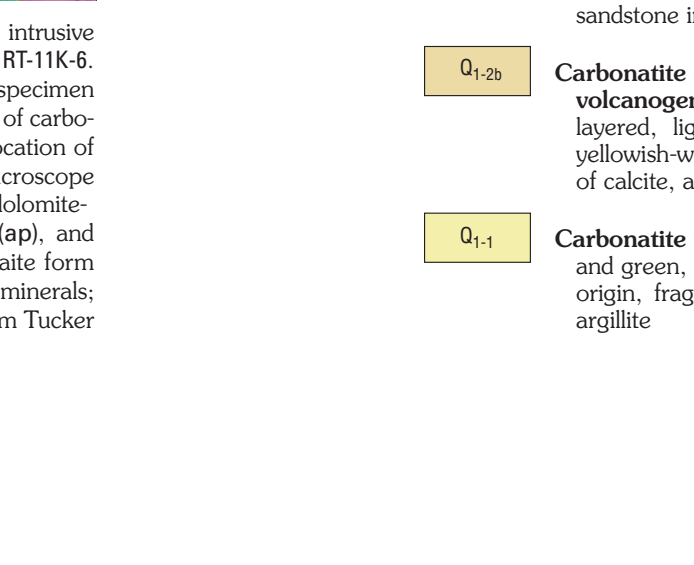
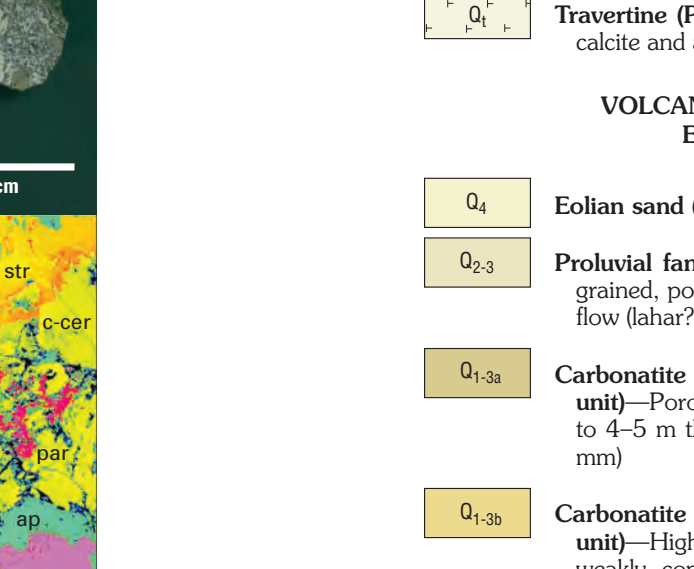
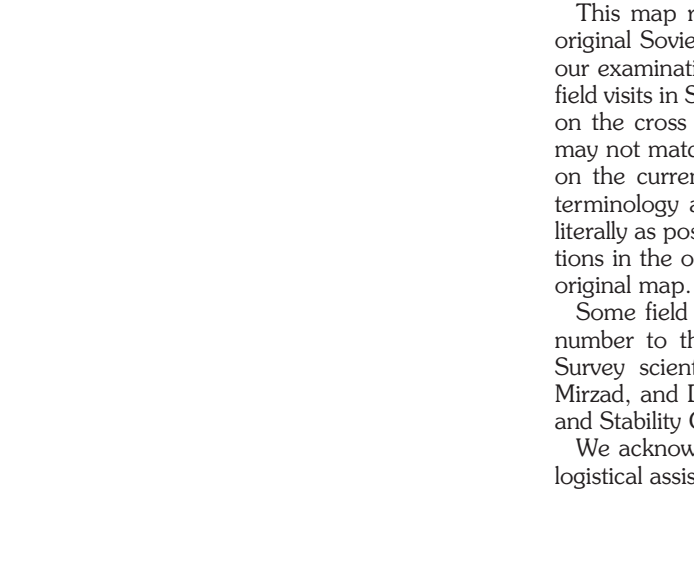
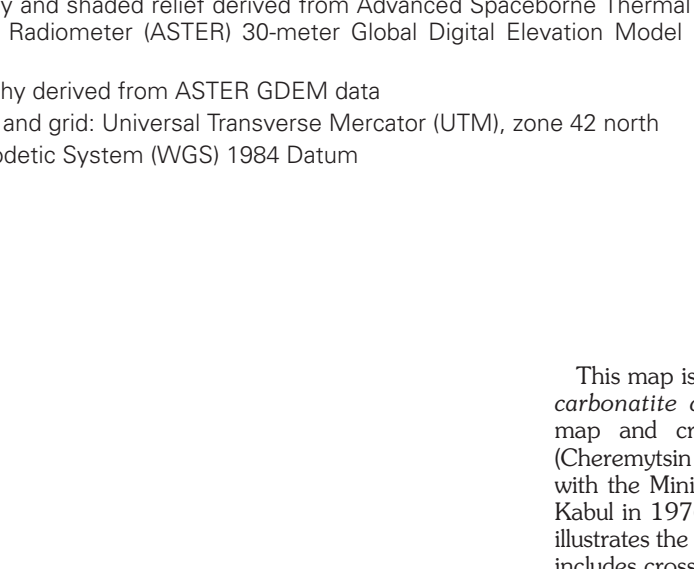


Figure 47—Close-up view of another Type 1 interbedded with an intrusive mass of fine-grained basalt, calcite, and dolomite. (Traverse no. 3)

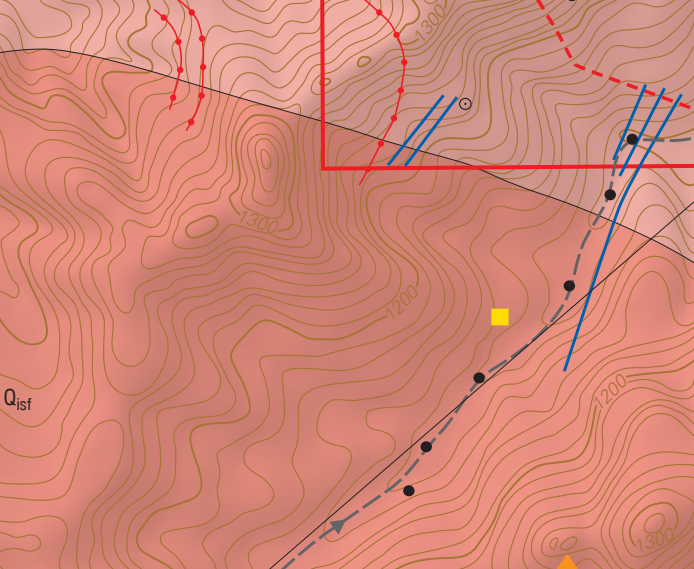


Figure 48—Tabular sheet, approximately 1.5 m thick, outlined by dashed line, of typical Type 2 interbedded showing very coarse-grained rare earth element (REE) enriched carbonate cutting finely bedded dolomite in the northeastern margin of the central intrusive vent. (Traverse no. 3)

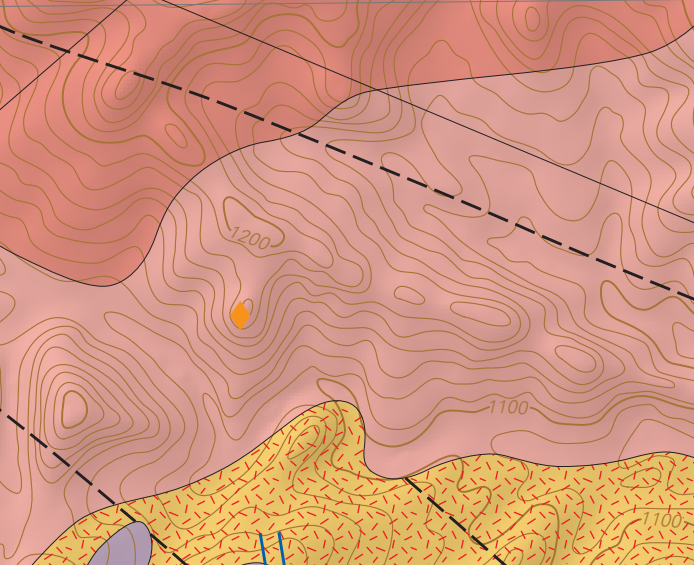


Figure 49—Close-up view of Type 2 interbedded in a coarse-grained carbonate dike. Note the coarse-grained igneous texture with dolomite crystals of barite, barite, and calcite, and the presence of dolomite, barite, and calcite. (Traverse no. 3)

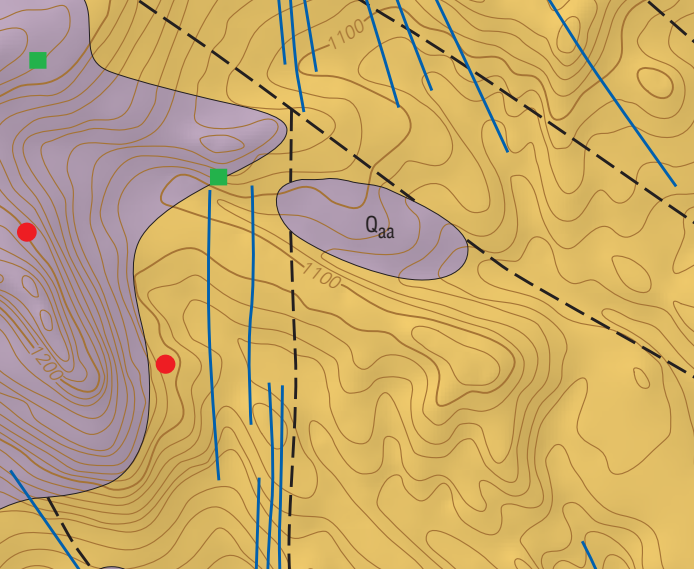


Figure 50—Close-up view of barite and dolomite (dolomite) in a granitic patch of Type 2 interbedded tabular sheet shown in Figure 18. Other visible interbeds include barite, barite, and calcite. (Traverse no. 3)

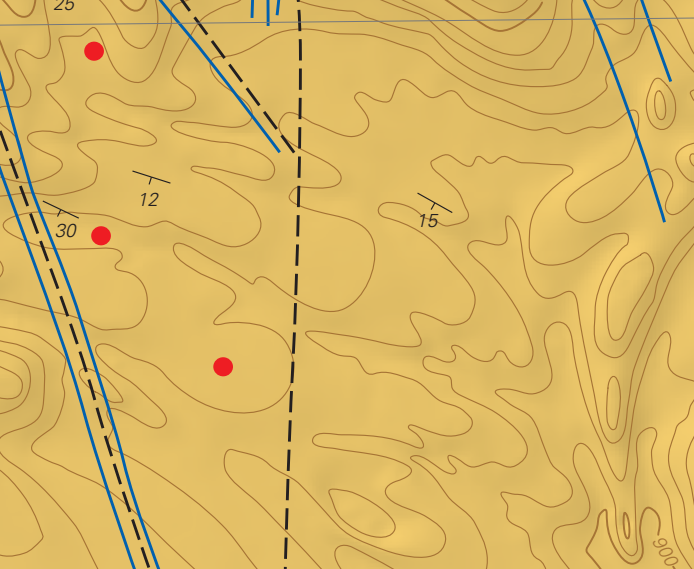


Figure 51—Hydrothermally altered rare earth element (REE) minerals of the Type 1 veins and disseminated pods in barite-sulfate dolomite, northeastern margin of the central intrusive vent. (Traverse no. 3)

